

Effect of metal temperature on the short contact time adhesion of molten poly(ethylene terephthalate)

Marco Carati^{a,b,*}, Maurizio Fiorini^c

^a Department of Electrical, Electronic, and Information Engineering "Guglielmo Marconi" - Alma Mater Studiorum – University of Bologna, Via Giuseppe Garibaldi 37, Imola (BO), 40026, Italy

^b Corporate Academy - SACMI Imola S.C., Via Selice Provinciale 17/a, Imola (BO), 40026, Italy

^c Department of Civil, Chemical, Environmental, and Materials Engineering - Alma Mater Studiorum – University of Bologna, Italy

ARTICLE INFO

Keywords:

Metal adhesion
Short contact time
poly(ethylene terephthalate) adhesion
Metal temperature
Preform compression
Molding technology
Aluminum alloy

ABSTRACT

This study focused on the effect of metal temperature on the short contact time (few milliseconds) adhesiveness of a molten poly(ethylene terephthalate) (PET) cylinder. Although such a short contact time is typical for PET cylinder handling during preform compression molding (an innovative technique which has many advantages over injection molding, such as higher sustainability, owing to the lower energy and raw material consumption), this type of PET–metal contact has not been examined in the literature. Therefore, a new experiment was designed to test two different metals: stainless steel (AISI 316) and an aluminum alloy (EN AW-6082-T6). Both metal surfaces were finished to achieve nearly identical roughness and morphology as measured by profilometers, while their contact angles were determined according to previous studies. Afterwards, a series of tests including more than 300 single contacts were performed to monitor several parameters affecting PET adhesiveness. The obtained results revealed that the two tested materials exhibited different properties and suggested a probable short contact time adhesion mechanism. This study may be used as reference in the selection of appropriate materials and temperature for molten PET cylinder handling tools. Moreover, since the described phenomenon was previously unknown to the scientific community, this research could be useful in many other research and industrial fields.

1. Introduction

Poly(ethylene terephthalate) (PET) is a commonly used thermoplastic polymer and one of the most frequently recycled polymers in the world [1]. PET is widely utilized in the packaging industry because of its physical and optical properties [2–7]. Nathaniel Wyeth patented a PET bottle in 1973 [8], and a two-stage stretch blow molding (SBM) process is arguably the most popular technique for manufacture PET bottles [9, 10]. The bottle production process starts with the dehumidification of PET pellets, which are subsequently extruded and injected into closed molds with a preform shape.

Some companies (SACMI, Toyo Seikan Group, Graham Packaging and others) are developing an alternative compression molding process to produce beverage preforms [11,12]. During this process, hot PET flows out of a nozzle after being melted inside an extruder, and a molten PET cylinder (henceforth referred to as a “gob”) is cut off from the melt

by a blade. The gob with a weight and shape depending on the preform type is handled and placed inside an open mold cavity (here, “handling” is defined as a process starting immediately after the gob cutting and ending after the gob insertion into the mold). Unlike injection molding, the mold in this technique remains open while the plastic is placed into the cavity, and its three parts (core, cavity, and neck rings) begin closing only after the gob enters the cavity at controllable speed and force. The closed mold shapes the gob into a preform, which is extracted by a gripper and cooled using a conformal cooling channel with a shape matching that of the cavity. Compression has many advantages over injection, including a lower energy consumption, a smaller amount of the raw material (PET), a higher weight homogeneity, and the ability to process preforms with relatively high intrinsic viscosities (IVs) and, therefore, relatively high degrees of orientation [13,14]. Moreover, rotating compression molding machines consume significantly lower energy when PET bottles are manufactured via a single-stage SBM

* Corresponding author. Department of Electrical, Electronic, and Information Engineering “Guglielmo Marconi” - Alma Mater Studiorum – University of Bologna, Via Giuseppe Garibaldi 37, Imola (BO), 40026, Italy.

E-mail address: marco.carati2@unibo.it (M. Carati).

<https://doi.org/10.1016/j.polymer.2023.126570>

Received 19 July 2023; Received in revised form 26 October 2023; Accepted 3 December 2023

Available online 7 December 2023

0032-3861/© 2023 The Authors. Published by Elsevier Ltd. This is an open access article under the CC BY license (<http://creativecommons.org/licenses/by/4.0/>).

process [11,12]. The main issues encountered during PET preform compression molding are related to the separation and especially handling (within a few tenths of a second) of the molten PET gob. Therefore, multiple patents on this topic have been filed by several companies (SACMI, Toyo Seikan Group, Graham Packaging and others) in recent years [15–18].

Polyethylene and poly(1-methylethylene) caps and containers have been produced for thirty years with compression molding technology, for example with the machines made by SACMI. The substitution of the aforementioned polymers with PET is not possible in the machines of the first generation: the production will not start or will stop after very few molding cycles because of polymer adhesion to the metal handling components. Therefore, industrial experience in compression molding has shown that the adhesion of PET to metal surfaces is significantly higher than those of other industrial polymers such as polyethylene and poly(1-methylethylene) and varies significantly with temperature and metal type. This confirms the findings of Dos Santos Ferreira et al. [19], who carried out a quantitative comparison of the adhesion in metal-to-plastic systems in the field of metallization of plastic films.

Technical solutions can reduce the molten PET gob/metal contact time to a few milliseconds during gob handling [20]. The handling tool metal alloys are often aluminum or stainless steel, endowed with an aluminum oxide or chromium oxide layer, respectively, to increase metal corrosion resistance.

The topic of metal-polymers adhesion was studied from many perspectives in the overmolding injection field both through mechanical metal surface modification to promote mechanical bonds interlocking and chemical metal surface modification [21–24].

Few works were devoted to measuring the adhesion strength of the steel–plastic interface, and the aim of most studies was to reduce plastic stickiness to steel dies during the forming process [25–27]. Notably, Shalnov et al. [26] and Chen et al. [27] performed surface morphology observations by atomic force microscopy to reduce plastic adhesion in the forming process by surface modification.

Interesting metal mold temperature effects were observed during thermoplastic bonding to metals via injection molding [28]. Because metallized plastic films are widely utilized in the packaging industry, many researchers have investigated the metal–polymer interfaces formed by thermally depositing metals onto polymer surfaces in vacuum to increase their adhesion [29–32]. However, certain conditions used in these works differ from those utilized in the present study (especially the vacuum deposition), indicating that the metals are not oxidized. Several researchers have developed new methods for preparing PET coatings on metal substrates for food and beverage containers [33–37]. In these methods, PET is hot-extruded directly onto a metal surface or laminated under combined heat and pressure conditions; however, their contact times are significantly longer than milliseconds. Finally, Al Maliki et al. examined the effect of cold plasma treatment on the adhesion-related PET surface chemistry and morphology (polymer/polymer and polymer/steel joints) to increase the adhesive shear rate [38].

In summary, studies on the aluminum/PET and stainless steel/PET adhesiveness in the contact time range of several milliseconds (typical for compression molding) are not present in existing literature. Therefore, this research has a great scientific significance, examining for the first time a phenomenon that is currently unknown to the scientific community and could arouse an interest in many research and industrial fields. This study proposes an innovative test to assess the effect of the metal wall temperature on PET adhesion within a very short contact time. The PET gob before contact is endowed with a speed characteristic of the compression molding handling process. The analyzed metal alloys are most frequently employed in automatic machines that produce packaging for the beverage industry; therefore, the findings of this study can also provide useful information for industrial applications.

2. Experimental

2.1. Test design

2.1.1. Test goals

The PET/metal adhesiveness is strongly dependent on the metal temperature and type. This phenomenon was observed by the authors while testing a prototype of an industrial machine with many uncontrolled parameters. In the industrial process the thermal capacity of the metal component in contact with the molten PET cylinder during gob handling is almost two orders of magnitude higher than that of the gob. As a consequence, given also the huge difference between the PET and the metal thermal effusivity (i.e. the ability of a material to exchange thermal energy with its surroundings) and diffusivity (i.e. the rate of transfer of thermal energy of a material from the hot end to the cold end), there is no considerable temperature variation on the metal during such a short contact time (several milliseconds).

The objective of this research study was to elucidate the short contact time PET/metal adhesion mechanism. The obtained results would provide information related to the effect of the metal temperature and the metal type on the short contact time PET metal adhesion, thus helping implement the cutting-edge PET compression molding technology on an industrial scale and opening new prospective scenarios of research in other scientific and industrial fields.

The conducted test included the analysis of PET gob adhesiveness within a short contact time (several milliseconds) to the clean surfaces of an aluminum alloy (EN AW-6082-T6) plate and stainless steel (AISI 316) plate with similar roughness and morphology. Each metal plate thermal capacity is similar to a typical gob handling tool one. Test particular aim was to verify that increasing metal plate temperature results in an “adhesion threshold temperature” that promotes PET gob bonding to the metal surface. Moreover, in case the adhesion threshold temperature exists, test goals were as follows.

1. To determine the adhesion threshold temperature for two different material types (stainless steel AISI 316 and aluminum alloy EN AW-6082-T6).
2. To verify whether the adhesion gradually decreases with decreasing temperature below the adhesion threshold temperature or is abruptly switched off.

2.1.2. Testing setup

The utilized testing setup consisted of the following parts (Fig. 1).

1. A PET dehumidification plant (DP620, Piovan, S. Maria di Sala, Italy) composed of a dehumidification tower (DPM605) and a hopper loader (C10D).
2. A single-screw PET extruder with a screw diameter of 25 mm, length-to-diameter ratio of 21, and four zones of independent thermal heating through electric resistances.
3. An oleo-dynamic syringe for collecting the PET flowing from the extruder and pushing it rapidly out of the nozzle.
4. A blade placed after the nozzle to separate gobs with a desired weight.
5. A by-pass nozzle to have the possibility to inspect the PET flow directly after the extruder.

The setup was designed to ensure that the gob hits the metal plate.

Each plate had a thermo-resistance and a temperature sensor (Pt100 sensing resistor) attached to its back surface opposite to the gob contact surface. The purpose of the sensor was to regulate the plate temperature in the vicinity of the gob contact area. The plate and its support were separated by a layer of a thermal insulating material to maintain uniform plate temperature to the extent possible. A proportional–integral–derivative (PID) thermoregulation controller regulated the temperature and allowed the operator to change it easily. Notably, the

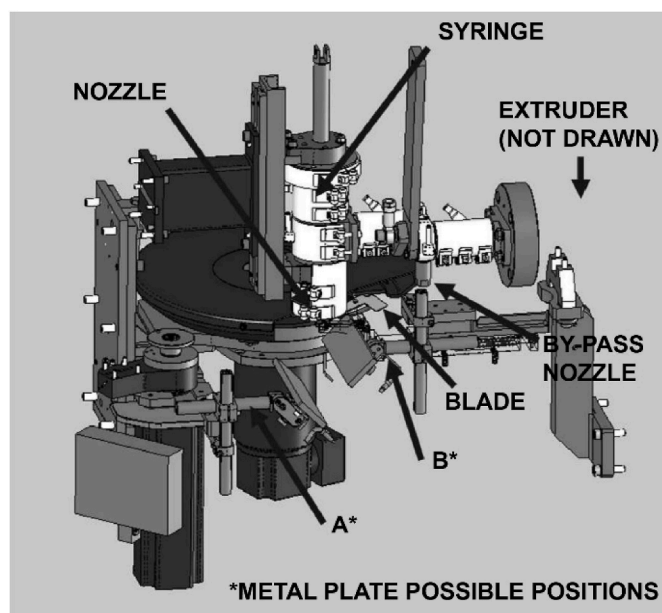


Fig. 1. Testing machine details of the cutting zone. A and B are two possible plate positions, of which B was chosen because the gob trajectory was more repetitive.

plate temperature in the precise gob contact area was measured with a contact thermocouple only after the test completion to avoid altering surface characteristics. After the plate temperature (regulated by Pt100 sensing resistor) reached the required equilibrium, five measurements were conducted using the contact thermocouple. For each measurement, the maximum and minimum temperatures of the thermoregulation cycle were recorded. Contact area temperature measurements were done at each temperature that were set on the thermoregulation controller during the test with the gobs.

2.1.3. Polymer properties and dehumidification parameters

PPK™ FR resin is a food grade PET copolymer resin based on terephthalic acid. It is a commercial material produced by Plastipak Italia which was used without any modifications, apart from drying. Its high clarity and sparkle make it suitable for the production of bottles and other containers by conventional single-stage and two-stage processing techniques. It is also of high molecular weight grade for manufacturing containers with an IV of $0.08 \pm 0.002 \text{ m}^3/\text{kg}$ (or, as is frequently reported [9,10,39,40], $0.8 \pm 0.02 \text{ dl/g}$) according to the ASTM D4603:03 standard. Moreover, the melting point of this resin is $249 \text{ }^\circ\text{C}$, and its acetaldehyde content declared by the manufacturer is below 1 ppm. A PET dehumidification procedure was performed in a Piovan dryer at $160 \text{ }^\circ\text{C}$ for 4 h prior to testing. The PET quantity in the drier was sufficient for few hours of testing.

2.1.4. Testing methodology

Before starting each test, the metal plate was accurately cleaned with a commercial multi-purpose cleaner spray (Z263, HASCO Hasenclever GmbH + Co KG, Lüdenscheid, Germany; its chemical composition is listed in Table 1) and clean soft cloth to avoid changing the plate surface.

Table 1
Chemical composition of the cleaning spray for the plate contact surface.

Chemical name	Concentration (% w/w)
1-Ethylpyrrolidin-2-one	25 to <50
Propan-2-ol	15 to <20
1-Methoxy-2-propanol	2.5 to <10
2-(3-Methoxypropoxy)propan-1-ol	10 to <25

The aim of the cleaning step was to eliminate traces of any previous contacts.

Eight parameters were recorded for each test: (1) if the gob stuck to the metal plate or bounced off the metal plate, (2) minimum and maximum electrical absorptions of the extrusion screw, (3) extruder inlet temperature, (4) air dew point, (5) air pressure, (6) air temperature and (7) air relative humidity (RH), (8) the weight of the gob (if the gob stuck to the metal plate). The second and third parameters were recorded because they helped detect short-period variations in the PET dehumidification conditions. The melt PET temperature and PET humidity were measured for every five gobs as they were significantly more time consuming. The utilized PET hygrometer was an AQUA-TRAC® system manufactured by Brabender Messtechnik (Duisburg, Germany). Measurements (accuracy: $\pm 10 \text{ ppm}$) were completed within 40 min, and the PET pellets were removed from the lower part of the PET drying hopper. Furthermore, a video (Photron FASTCAM-ultima APX (Tokyo, Japan)) was recorded during each test at a frame rate of 2000 fps, which represented a compromise between the image quality, information obtained, and file size. The video described the gob cutting and bouncing processes until the gob either left the video area or stuck to the metal plate.

2.2. Metal surface characterization

2.2.1. Roughness

The reduction in the PET mold adhesion reported in the literature suggests that roughness is an important parameter for a single adhesion contact test; however, the related tests were conducted at long contact times (hours) [26]. In the present study, the effect of the metal surface roughness on the short contact time adhesiveness was not investigated. To mimic the industrial conditions during testing, an industrial rough surface was preferred over a polished one. Because the elastic moduli and general mechanical properties of the two materials are different, they differently respond to plastic deformation. Hence, the machining process was optimized to produce similar levels of roughness and morphology. An opto-mechanical system (HOMMEL-ETAMIC Nanoscan 855, Jenoptik AG, Jena, Germany) and a 3D optical surface profiler with coherence scanning interferometry technology (NewView™ 9000, Zygo Corporation, Middlefield, Connecticut) were used for roughness and morphology measurements, respectively.

2.2.2. Contact angle

Surface free energy (SFE) is employed to assess the chemical pre-disposition of a surface to create polar or dispersive bonds. SFE is usually [41,42] measured indirectly by the Owens, Wendt, Rabel, and Kaelble method using sessile drop contact angles of at least two liquids with known dispersive and polar components of the surface tension, wherein at least one of these liquids contains a polar group [43–45]. Although certain studies have shown that the absolute value of SFE depends on both the calculation method and compositions of the probe liquids, the SFEs of two metals can be directly compared if their calculations are conducted using the same method, and the same liquids (a dissimilar liquid pair) are used for contact angle measurements (and their values are below 110°) [46,47]. Based on previous studies [41,42,48], the liquids used for this purpose included bi-distilled water, which met the specifications for water type 2 (ISO:3696:1987, "Water reagent for use in laboratory analysis") according to the supplier datasheet, and diiodomethane (CH_2I_2 ; purity $\geq 98.5 \%$).

Contact angle tests were performed in a laboratory on a KRUSS DSA30S tensiometer (Hamburg, Germany) using a static sessile drop technique at room temperature ($24 \text{ }^\circ\text{C}$) and RH between 37 and 52 %, which were similar to the conditions utilized in previous studies [26,49]. Notably, the literature values of contact angle (and thus SFE) determined for aluminum alloy and AISI316 stainless steel at surface temperatures between room temperature and $120 \text{ }^\circ\text{C}$ were almost constant [50,51].

2.3. Modeling adhesiveness variation with metal temperature

One of the aims of the designed test was to verify whether, below the adhesion threshold temperature (if present), adhesion decreases with decreasing temperature following any mathematical law or if the adhesion represented an on-off process activated at a threshold temperature.

The innovative idea of the described test is to try to correlate the variation (if present) of the adhesion at different plate temperature to the variation (if present) of the gob energy, in particular gob mechanical energy (E_{mec}) before and after the gob contact with the plate.

Gob mechanical energy is composed by its gravitational potential energy and its kinetic energy and can be expressed as follows:

$$E_{mec} = K + E_{pot} \quad (1)$$

where K is the gob kinetic energy and E_{pot} is the gob gravitational potential energy.

The gob translates and rotates around its center of mass, therefore its kinetic energy is composed of a translation component K_T and a rotational component K_R , as follows:

$$K = K_T + K_R \quad (2)$$

The translation component K_T of the gob kinetic energy is expressed as follows:

$$K_T = 0.5 m_g \cdot (v_C^2) \quad (3)$$

where m_g is the gob mass measured with a XP205 (Mettler Toledo, Columbus, Ohio, USA) analytical balance with a readability of 0.00001 g, a repeatability at low load (lower than 10 g) of 0.000015 g and a linearity deviation of 0.0001 g (these values are the limit values, typical values are lower); v_C is the velocity of the gob center of mass before the gob-plate contact.

The rotational component K_R of the gob kinetic energy is expressed as follows:

$$K_R = 0.5 \omega^T \times I_c \times \omega \quad (4)$$

where ω is the gob angular velocity vector; ω^T is the transpose of ω ; \times is the mathematical operator for the vector product; I_c is the gob tensor of inertia related to the gob center of mass.

If the gob rotates around one of its three principal axes of inertia, Eq. (4) can be expressed as follows:

$$K_R = 0.5 I \cdot \omega^2 \quad (5)$$

Where I is the gob moment of inertia around its rotation axis (one of its three principal axes of inertia), ω the gob angular velocity.

In this section, all variables and parameters obtained before the gob touches the metal are described by subscript 1, while those determined after the gob detaches from the plate are described by subscript 2. Gravitational potential energy is almost constant between an instant before and an instant after the contact with the plate. Therefore, Eq. (1) can be expressed as follows:

$$\Delta E_{mec12} \simeq \Delta K_{12} \quad (6)$$

where ΔE_{mec12} is the difference in the gob mechanical energy before and after the gob contact with the plate and ΔK_{12} is the difference in the gob kinetic energy before and after the gob contact with the plate.

In the following lines some considerations about the gob contact with the metal plate in the designed test are reported.

A fraction (E_{mbc}) of the gob kinetic energy before contact may be used by the PET chains to enter the cavities of the metal surface to create mechanical bonds (if they are present). Mechanical bonds interlocking (named also mechanical interlocking) is one of the polymer/metal adhesion mechanisms [28].

In a recent paper Zou et al. [52] focused on clarifying the underlying bonding mechanisms of laminated chromium-coated steel strip from the microscale to the molecular scale. Microscale mechanical interlocking may play a role, for example when polymer film and metal strip are laminated together by application of a pressure which favors diffusion of macromolecules into the rough metal interface. In addition to this, chemical bonding, such as hydrogen bonding between hydroxyl groups deriving from metal oxide and oxygen atoms from the carbonyl groups in PET ester bonds, has a more prominent role. Zou et al. [52] suggested the formation of mono- and bidentate complexes characterized by $-(O=)C-O-Cr$ and $-C-(O-Cr)_2$ bonding.

PET is a viscoelastic material that exhibits both viscous and elastic characteristics during deformation and its viscosity increases with temperature decrease [53–57]. Accordingly, the gob kinetic energy can decrease after the gob-metal contact because some energy (W_{vis}) is dissipated during contact owing to the viscous characteristics of PET and this energy can vary with gob overall temperature (T), therefore $W_{vis}(T)$.

Furthermore, the gob theoretically releases thermal energy during contact owing to the temperature difference between the gob and the plate. Moreover, if chemical bonds are formed at the metal-gob interface, thermal energy is released.

The work of adhesion (W_{ad}) is the work that must be performed to separate two adjacent phases on either side of the liquid-solid phase boundary. From a physical point of view, the work of adhesion represents the energy required to break mechanical or chemical bonds.

Accordingly, the difference in the gob kinetic energy before and after the gob contact with the plate can be expressed as follows:

$$\Delta K_{12} = E_{mbc} + W_{vis}(T) + W_{ad} \quad (7)$$

It is important to be aware that PET exhibits a very low thermal conductivity and diffusivity and that the contact lasts for a very short time ($\sim 10^{-3}$ s). Therefore, the overall gob temperature just before contact, during the contact with the aluminum alloy (EN AW-6082-T6) or stainless steel (AISI 316) and in the first milliseconds after it, can be considered almost the same.

Moreover, given the constancy of the gob speed and trajectory before contact, it is reasonable to affirm that the energy dissipated during contact owing to the viscous characteristics of PET remains almost constant during the test campaign. Therefore, Eq. (7) can be expressed as follows:

$$\Delta K_{12} \simeq E_{mbc} + W_{ad} + A \quad (8)$$

where A is a quantity ($W_{vis}(T)$) which is almost constant in the test conditions as described in the previous lines.

In the conducted test, designed to replicate the gob handling state of art in the PET compression molding technology, the adhesion energy (E_{ad}) can be defined as the sum of the energy required for the creation of mechanical bonds (if they are present) between the PET gob and the metal plate and of the work of adhesion required to separate the PET phase from the metal phase, as follows:

$$E_{ad} = E_{mbc} + W_{ad} \quad (9)$$

Therefore, given Eq. (8), the adhesion energy can be expressed as follows:

$$E_{ad} \simeq \Delta K_{12} - A \quad (10)$$

In the comparison of tests conducted at different plate temperature, if the gob possesses less kinetic energy when bounced off the metal plate, the adhesion increases. Moreover, if the adhesion energy exceeds the available kinetic energy, the bonds between the gob and the metal plate remain intact.

Given Eq. (2), the difference in the gob kinetic energy before and after the gob contact with the plate can be expressed as follows:

$$\Delta K_{12} = \Delta K_{T12} + \Delta K_{R12} \quad (11)$$

where ΔK_{T12} is the difference in the translation component of the gob kinetic energy before and after the gob contact with the plate and ΔK_{R12} is the difference in the rotational component of the gob kinetic energy before and after the gob contact with the plate.

Given Eq. (3), the difference in the translation component of the gob kinetic energy before and after the gob contact with the plate can be calculated as follows:

$$\Delta K_{T12} = 0.5 m_g \cdot (v_{C1}^2 - v_{C2}^2) \quad (12)$$

The difference in the rotational component of the gob kinetic energy before and after the gob contact with the plate can be expressed as follows:

$$\Delta K_{R12} = K_{R1} - K_{R2} \quad (13)$$

where K_{R1} and K_{R2} can be calculated in two different ways, i.e. generally according to Eq. (4) or, if the gob rotates around one of its three principal axes of inertia, more easily according to Eq. (5).

Tracker©, a free video analysis and modeling software, was used to determine gob trajectories and speeds.

2.4. Testing parameters

Several minutes pass between different tests. Each time the syringe ejects the melt, the exposed section of the melt is discarded by cutting off the molten PET cylinder (henceforth referred to as a "scrap gob"). In the industrial process, the gob is cut very frequently (every 0.05–0.8 s depending on the machine productivity). The purpose of the tests conducted in this study was to reproduce industrial conditions as closely as possible. Certain properties (such as surface temperature) of the cut molten PET surface can significantly change owing to the prolonged air exposure (minutes versus tenths of seconds) after exiting the nozzle. A plate position (position B of Fig. 1) that (1) maintains the cleanliness of the plate surface by preventing the scrap gob from falling on the metal plate and (2) ensures high repeatability of the gob trajectory has been determined. After the initial setup, the blade speed was kept constant in all tests.

High repeatability of the gob trajectory was achieved at a gob weight of 4 g, where the difference between two different trajectories before impact was below 2 mm. Before the contact with the metal plate, the gob rotation axis passed through the gob center of mass and was perpendicular to the molten cylinder (gob) axis, therefore its rotational kinetic energy can be easily determined through Eq. (5). Notably, the high-speed camera was placed perpendicularly to the plane of the gob path before contact.

A thermal simulation was performed to estimate the temperature on the gob surface that touches the metal plate. This surface is created by the blade that separates the gob from the melt inside the nozzle. The utilized software was the ANSYS® FEM (Finite Element Method) thermal transient module, and the melt temperature inside the nozzle was set to 275 °C (the average measured temperature). The simulation procedure included several time steps each with its own parameter values; it was initiated at the time of the melt ejection from the nozzle and ended before the gob touched the plate. In the first part of the simulation, the upper surface of the gob remained in contact with the melt inside the nozzle at a constant temperature maintained by the thermo-resistances, while the lower and lateral melt surfaces were exposed to air and released thermal energy through natural convection and radiation. In the second step, the gob was cut off; the upper surface was created by the blade; and the gob started moving; as a result, natural convection was replaced by forced convection. Furthermore, both convection and radiation occurred on the gob upper surface. All the thermal parameters were calculated according to related studies [58,59]. The average temperature (not the temperature on the microscale) of the gob

surface just before the contact with the metal plate was 2–4 °C lower than that of the melt inside the nozzle (this range resulted from the uncertainty of the heat exchange with the blade during gob cutting).

3. Results and discussion

3.1. Introduction

A total of 341 valid tests have been conducted. Among them, 180 tests were performed for AISI 316 stainless steel (87 gobs stuck, and 93 gobs bounced), and 161 tests were conducted for the EN AW-6082-T6 aluminum alloy (76 gobs stuck, and 85 gobs bounced). An analysis of more than 50 random videos confirmed high repeatability of the gob trajectories. After the tests were completed, prior to the measurements of the precise gob contact area temperature (see section 2.1.2), the plate roughness and morphology of the contact area were examined; the obtained values were identical to those determined at the beginning of the tests. The calculated percentage deviation of profile roughness parameters (Ra, Rt, Rz) is less than 10 %. Figs. 2 and 3 show the plates morphology.

The obtained results (Table 2) about contact angle revealed a slight difference (approximately 3 mN/m) between the SFEs of the rough and polished surfaces, which was consistent with the results of a previous study on the effect of the metal surface roughness on the wettability of aluminum and steel alloy conducted by Kubiak et al. [49].

The SFE difference between the two rough surfaces was almost insignificant (1 mN/m, lower than the measurement uncertainty) owing to the stainless steel slightly larger polar component. Thus, it has been concluded that rough surfaces have nearly equal chemical predispositions to creating polar or dispersive bonds.

3.2. Effect of plate temperature

After the first several days of testing, a certain temperature range in which the gobs randomly bonded or bounced was identified. Hence, the highest temperature, at which all gobs bounced, and when possible, the lowest temperature, at which all gobs bonded were measured every day. This necessitated repeated tests at the same plate temperature multiple times on different days and at different times during the day, with the purpose to increase the number of samples and confirm that the observations were not dependent on other parameters. The minimum temperature interval between the tests was fixed at 5 °C. Apart from a few exceptions, at least five tests were performed daily for each temperature to obtain statistics. For each material, the plate starting temperature was chosen in the temperature range in which the gobs randomly bonded or bounced.

Fig. 4 describes the gob behaviors observed after the contact with the aluminum and stainless-steel plates in the temperature range of 50–135 °C. The highest temperature, at which the gobs did not stick to the metal plate, named "adhesion threshold temperature" was considerably different for the two tested plates. This difference of 11.7 ± 2.2 °C (derived from Table 3) remained remarkably high even in the worst-case scenario, i.e. 9.5 °C considering the stainless steel highest temperature, the aluminum alloy lowest temperature and the temperature measuring system repeatability error (± 0.2 °C). Note that the same temperature measuring system was used for the two plates, therefore its accuracy (± 1 °C) has no influence on the aforementioned temperature difference.

Fig. 4 illustrates a particular phenomenon: the difference (15.8 ± 2.5 °C) between the lowest temperatures, at which all gobs stick to the EN AW-6082-T6 and AISI 316 plates (Table 4 is equivalent to Table 3). This phenomenon is less pronounced than the previous one because only two gobs out of 65 stuck on the AISI 316 surface at temperatures exceeding 115 °C. Because no data were available for EN AW-6082-T6 at 115 °C, this temperature was disregarded in this study. One gob (labelled A) stuck at 120 °C, the other (labelled B) at 130 °C. Their weights, videos (trajectories, motion laws, and contact times), and other

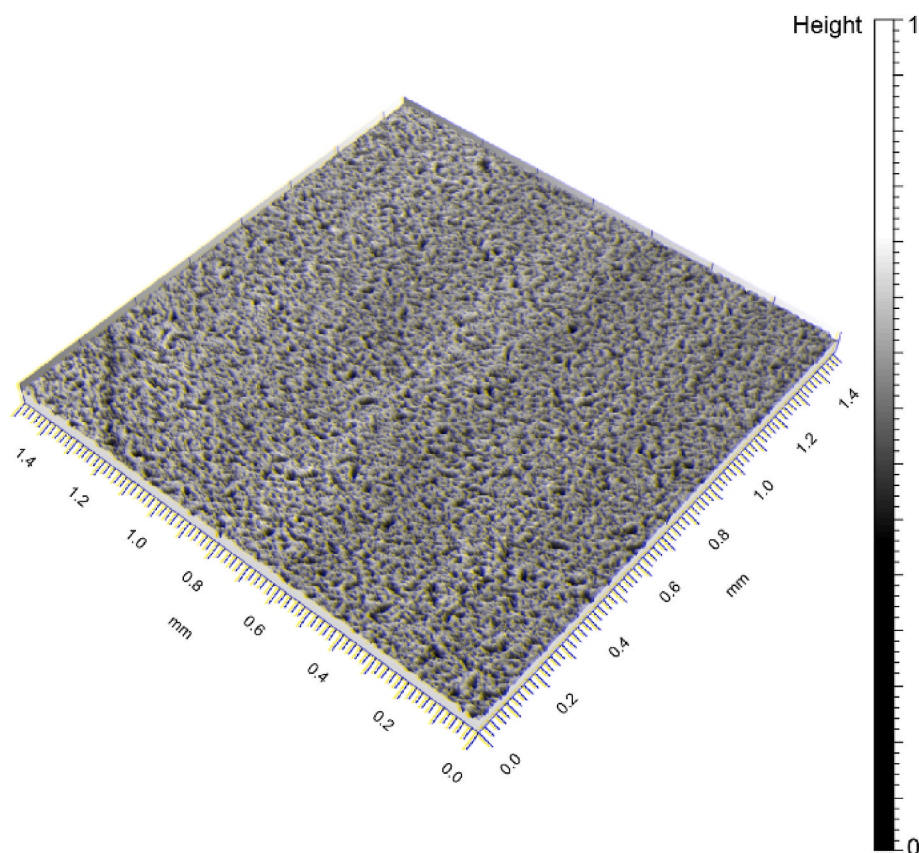


Fig. 2. 3D morphology of the EN AW-6082-T6 aluminum alloy plate with the measured area having the dimensions 1.5×1.5 mm. The color refers to the height of the surface in each point, and the height values are normalized in accordance with SACMI intellectual property policy.

characteristics (air dew point, RH, electrical absorption of the extrusion screw, extruder inlet temperature, melt temperature, and PET moisture content) were examined accurately. The only significant difference was observed for the contact time of gob B, which lasted from 0.0045 to 0.0050 s and exceeded the contact time obtained for the other samples by 50 %. This result is indicative of an exceptional situation and after bouncing, the gob moved away from the plate like the rest.

3.3. Influences of various parameters on the Poly(ethylene terephthalate)/metal adhesiveness

During each test, the impacts of various parameters on the PET/metal adhesiveness were determined at different plate temperatures. The most significant factors are discussed below.

3.3.1. Poly(ethylene terephthalate) moisture content

The water contents of PET pellet measured during testing (≤ 50 ppm) did not influence the gob adhesiveness. Similarly, variations in the measured values of the extrusion screw electrical absorption and extruder inlet zone temperature did not influence the test results.

3.3.2. Melt temperature

During testing, the PET melt temperature varied from 271 to 280 °C (measuring system accuracy, ± 1 °C; repeatability, ± 0.2 °C). The obtained data indicated that this variation did not affect the test results.

3.3.3. Gob mass

Almost all the stuck gobs masses (~ 150) and many of the bounced gobs ones were weighed, and the obtained gob mass variability ($< \pm 1$ %) had no effect on the PET/metal adhesiveness.

3.3.4. Air dew point, RH, pressure and temperature

During test campaign chamber air dew point varied between 5 and 18 °C, RH between 14 and 37 %, chamber air pressure and temperature between 98600 and 102400 Pa and between 29 °C and 48 °C, respectively. The obtained data indicated that the chamber RH, pressure and temperature variations did not affect the test results. For a certain plate temperature (110 °C), the lower air dew points resulted in gob bonding/sticking to metal plate; however, the data obtained for the two metals were contradictory and the quantity of the samples at this temperature is too scarce to get a general rule. Therefore, additional studies must be conducted to determine if there is a relationship between the air dew point and the PET/metal adhesiveness.

3.4. Adhesiveness below the sticking temperature

To clarify whether the PET adhesion to the metal surface decreases with decreasing temperature below the adhesion threshold temperature or follows an on-off mechanism, analysis (see section 2.3) was performed in the temperature range where the gob-metal adhesion did not occur.

The time passed between the gob cutting and impact was the same for all gobs and equal to 0.0115 ± 0.0005 s. The precision indicated is attributed to the selected camera frame rate. The results of the tests indicated that the gob contact with the metal plate from the moment it started touching the metal plate until the moment when none of its edges touched the plate lasted 0.0030 ± 0.0005 s. The gob dimensions and weight were measured separately. In the molten state, the gob diameter was ~ 16 mm, while the gob length was ~ 19 mm.

For each test, before the contact with the metal plate, the gob rotation axis passed through the gob center of mass and was perpendicular to the molten cylinder (gob) axis, therefore its rotational kinetic energy can

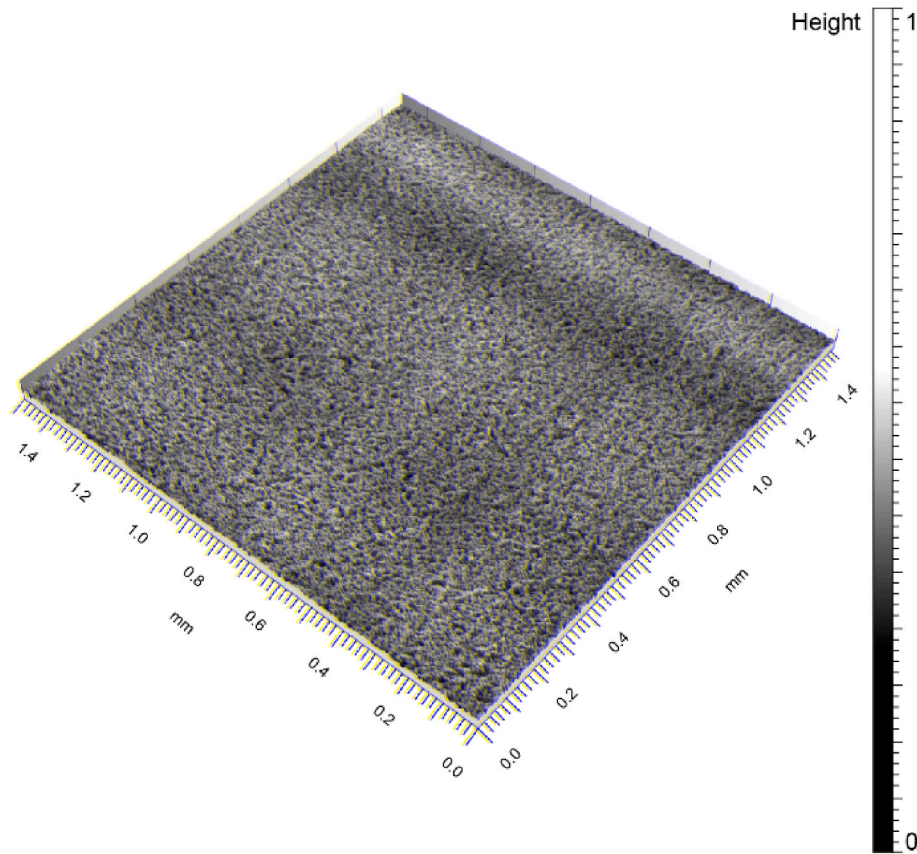


Fig. 3. 3D morphology of the AISI 316 stainless steel plate with the measured area having the dimensions 1.5×1.5 mm. The color refers to the height of the surface in each point, and the height values are normalized in accordance with SACMI intellectual property policy.

Table 2

Contact angle and SFE values obtained for the aluminum alloy and stainless-steel surfaces. The numbers of valid tests are listed in the brackets.

		Aluminum alloy EN AW-6082-T6		Stainless steel AISI 316	
		1B (Polished)	1A (Rough)	1B (Polished)	1A (Rough)
Average contact angle (°)	Bi-distilled water	79.7 ± 1.9 (7)	72.4 ± 2.1 (8)	79.1 ± 2.5 (7)	69.6 ± 2.9 (8)
	Diiodomethane	42.4 ± 0.6 (8)	42.9 ± 1 (9)	41.9 ± 1.4 (8)	43.1 ± 1.2 (8)
	SFE (mN/m)				
Dispersive component		38.4 ± 0.3	38.2 ± 0.5	38.6 ± 0.7	38.0 ± 0.6
	Polar component	3.8 ± 0.6	6.8 ± 0.9	4 ± 0.9	8.1 ± 1.4
	Total	42.2 ± 0.9	45.1 ± 1.5	42.6 ± 1.6	46.1 ± 2

be determined through Eq. (5), i.e. $K_R = 0.5 I \cdot \omega^2$. After the gob bounced off the metal plate, its rotation axis was no more one of the gob principal axes of inertia, therefore its rotational kinetic energy can be determined through Eq. (4), i.e. $K_R = 0.5 \omega^T \times I_C \times \omega$. The difference in the translation component of the gob kinetic energy before and after the gob contact with the plate is expressed by Eq (12), i.e. $\Delta K_{T12} = 0.5 m_g \cdot (v_{C1}^2 - v_{C2}^2)$ while the difference in the rotational component of the gob kinetic energy before and after the gob contact with the plate expressed by Eq. (13), i.e. $\Delta K_{R12} = K_{R1} - K_{R2}$. Therefore, the difference in the gob kinetic energy before and after the gob contact with the plate expressed by Eq. (11), i.e. $\Delta K_{12} = \Delta K_{T12} + \Delta K_{R12}$, can be calculated as follows:

$$\Delta K_{12} = 0.5 m_g \cdot (v_{C1}^2 - v_{C2}^2) + 0.5 I_1 \cdot \omega_1^2 - 0.5 \omega_2^T \times I_C \times \omega_2 \quad (14)$$

where I_1 is the gob moment of inertia around the gob rotation axis (one of its three principal axes of inertia) before the gob–plate contact.

Figs. 5 and 6 show the gob images captured before and after the contact with the metal plate, respectively, with the trajectories and speeds of its center and one of its edges.

The speed vector of the gob center of mass after the gob bounced off the metal plate (v_{C2}) predominantly lies in the plane perpendicular to the camera lens axis (within at least ~ 0.002 s after the gob detachment), therefore it can be measured with a small error. Unfortunately, after the gob bounced off the metal plate, its rotation axis was no longer parallel to the high-speed camera lens axis, therefore it is difficult to estimate the angular speed after contact (ω_2) of Eq. (14) ($\Delta K_{12} = 0.5 m_g \cdot (v_{C1}^2 - v_{C2}^2) + 0.5 I_1 \cdot \omega_1^2 - 0.5 \omega_2^T \times I_C \times \omega_2$). Before impact (Fig. 5), the speed of the gob center of mass (v_{C1} in Eq. (14)) was ~ 7 m/s, its rotation axis was one of the gob principal axes of inertia and gob angular speed (ω_1 in Eq. (14)) was ~ 600 rad/s. The rotational component of the kinetic energy (Eq. (5)) before impact ($0.5 I_1 \cdot \omega_1^2$) was approximately equal to one third of the translation component of the kinetic energy (Eq. (3)) before impact ($0.5 m_g \cdot (v_{C1}^2)$). Therefore, to evaluate the gob adhesion behavior below the sticking temperature, analysis was limited to the first part of Eq. (14) ($\Delta K_{12} = 0.5 m_g \cdot (v_{C1}^2 - v_{C2}^2) + 0.5 I_1 \cdot \omega_1^2 - 0.5 \omega_2^T \times I_C \times \omega_2$), i.e. the difference in the translation component of the kinetic energy ($\Delta K_{T12} = 0.5 m_g \cdot (v_{C1}^2 - v_{C2}^2)$) according to Eq. (12). Note that the Tracker© automatic trajectory detector did not function properly owing to the PET gob transparency and reflections. Therefore, for each video, the exact gob center of mass was manually selected, thereby introducing a small margin of error. To increase the measurement precision, v_{C1} was computed as the average of the last three speed values before contact and v_{C2} as the average of the first three speed values after contact.

The extreme values of the temperature ranges, in which no gobs stuck to the plate, were determined first to estimate the maximum

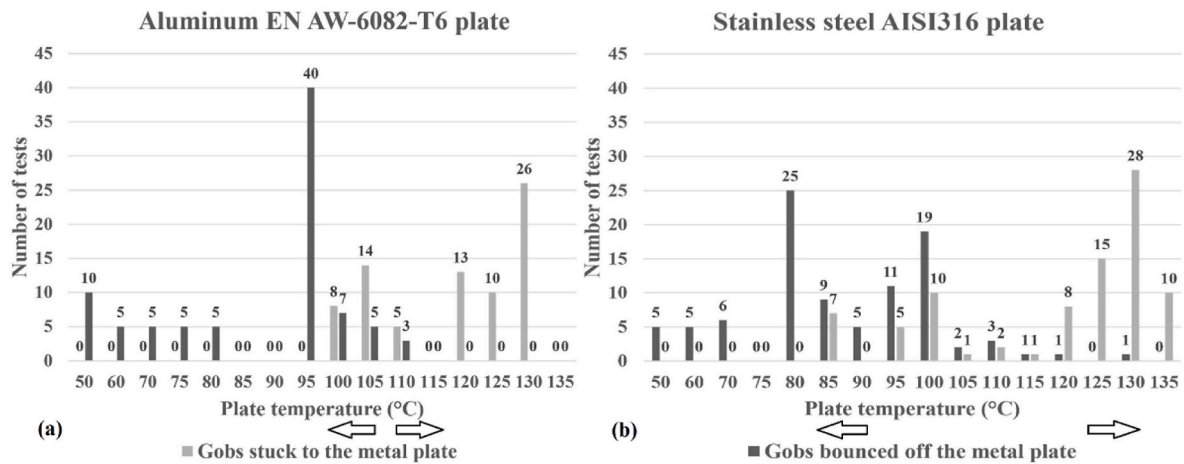


Fig. 4. Numbers of gobs that stuck and bounced off the (a) EN AW-6082-T6 aluminum and (b) AISI 316 stainless steel plates. The x-axis represents the temperature set on the thermoregulation device, and the white arrows highlight the changes in the test results. The numbers of gobs that bounced (dark grey) and remained stuck (light grey) are also listed for each temperature and plate material.

Table 3

Highest temperatures at which the gobs do not stick to the metal plate.

	Highest temperature, at which all gobs bounce (°C)	
	Aluminum alloy EN AW-6082-T6	Stainless steel AISI 316
Temperature set on the thermoregulation device	95	80
Highest temperature in the contact area	93.2	81.7
Lowest temperature in the contact area	91.2	79.3

Table 4

Lowest temperatures at which all gobs stick to the metal surface.

	Lowest temperature, at which all gobs stick (°C)	
	Aluminum alloy EN AW-6082-T6	Stainless steel AISI 316
Temperature set on the thermoregulation device	120	135
Highest temperature in the contact area	116.3	132.7
Lowest temperature in the contact area	114.5	129.6

variation. The obtained results (Fig. 7) suggest that the PET adhesion to the metal surface do not decrease with decreasing temperature below the adhesion threshold temperature but follows an on-off mechanism.

For AISI 316, there is no relevant variation in the gob speed difference between 50 °C and 80 °C. Meanwhile, from the gob speed measurements for EN AW-6082-T6, the adhesion appeared to increase slightly at low plate temperatures.

However, taking into account the gob speed standard deviation and the approximations previously reported, i.e. using Eq. (12) ($\Delta K_{T12} = 0.5 m_g \cdot (v_{C1}^2 - v_{C2}^2)$) instead of Eq. (14) ($\Delta K_{12} = 0.5 m_g \cdot (v_{C1}^2 - v_{C2}^2) + 0.5 I_1 \cdot \omega_1^2 - 0.5 \omega_2^2 \times I_C \times \omega_2$) and not considering the smallest component of the gob center of mass speed vector (v_{C2}) after the gob bounced off the metal plate, it is reasonable to assess that no significant differences were observed between the two samples.

Moreover, gob contact times were measured at the extreme values of the temperature ranges, where none of the gobs stuck to the plate. As anticipated, the same contact time (0.0030 ± 0.0005 s) was obtained for

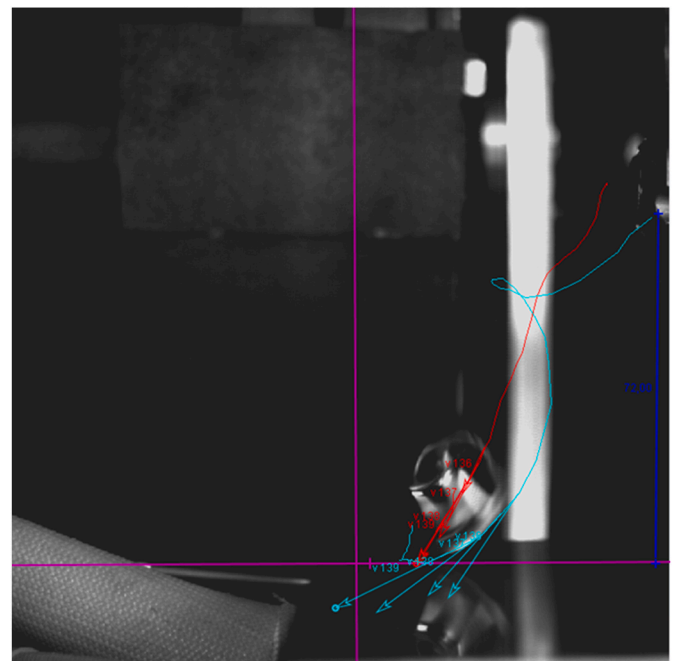


Fig. 5. High-speed image of the gob obtained before the contact with the metal plate. The image is rotated by 90° in the clockwise direction. In the upper part on the right there is the nozzle. The red/dark (the color reported after the slash refers to the image printed without colors) line starts at the nozzle center, while the cyan/light one starts at the nozzle lower edge. The blue/grey quote measures 72 mm. This is the distance between the lower edge of the nozzle and the plate contact plane. The red/dark line and the red/dark arrows represent the gob center of mass trajectory and velocity (v_{C1} in Eq. (14)), respectively. The cyan/light line and the cyan/light arrows represents the gob edge trajectory and velocity, respectively. The speed of the edge (cyan/light arrows) divided by the distance between the edge and the gob center gives the gob angular velocity (ω_1 in Eq. (14)). Trajectories (lines) and velocities (arrows) are shown for a qualitative interpretation (speed measurements were performed by the Tracker© tool). Each arrow is named with the letter “v” followed by a number. The number after the letter is related to a certain video frame and it increases with frame increasing. The time distance between two consecutive arrows/frames is 0.0005 s. Only arrows v136, v137, v138 and v139 are displayed to help figure clarity. They represent the last 1.5 ms before the gob contact with the metal plate. The vertical and horizontal purple/grey lines in the middle of the pictures can be ignored.

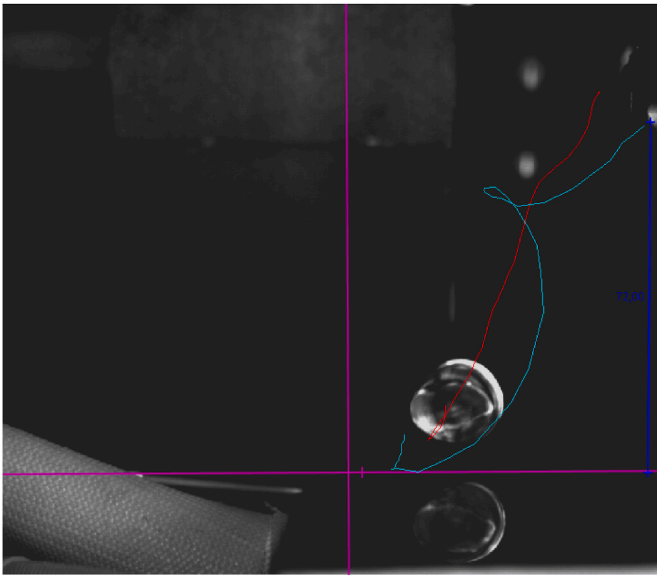


Fig. 6. High-speed image of the gob obtained after bouncing off the metal plate. The image is rotated by 90° in the clockwise direction. In the upper part on the right there is the nozzle. The red/dark (the color reported after the slash refers to the image printed without colors) line starts at the nozzle center, while the cyan/light one in its lower edge. The blue/grey quote measures 72 mm. This is the distance between the lower edge of the nozzle and the plate contact plane. The vertical and horizontal purple/grey lines in the middle of the pictures can be ignored. The red/dark line represents the gob center of mass trajectory. The cyan/light line represents the gob edge trajectory. Trajectories (lines) are shown for a qualitative interpretation. Before the contact (Fig. 5), the gob rotates around an axis parallel to the high-speed camera lens axis. After the contact, the gob starts rotating around an axis that is no longer parallel to the camera lens axis.

both the AISI 316 and EN AW-6082-T6 plates, and no differences were observed in the temperature ranges of 50–80 °C for stainless steel and 50–95 °C for the aluminum alloy.

Therefore, the adhesion process apparently followed the on-off

mechanism activated beyond a certain temperature (adhesion threshold temperature), which was typical for the studied plate materials.

To obtain more accurate data, future tests should use at least two (three give the highest precision) high-speed cameras or a high-speed camera with at least two (three give the highest precision) heads/lenses. This will allow the calculation of all the components of Eq. (14) ($\Delta K_{12} = 0.5 m_g \cdot (v_{C1}^2 - v_{C2}^2) + 0.5 I_1 \cdot \omega_1^2 - 0.5 \omega_2^T \times I_C \times \omega_2$) in a very precise way.

3.5. Short contact time adhesiveness model

The gob contact time with the metal plate was ~ 0.003 s, suggesting that conventional plastic-to-metal adhesion could not occur within the specified timeframe because this process would take up to several seconds. Moreover, according to the results of previous studies [50,51], the chemical predispositions of the studied surfaces to create polar or dispersive bonds were almost equal at the highest temperature, at which all gobs bounced.

The temperatures, at which the gobs started to adhere to the metal plates, were equal to ~ 80 °C for AISI 316 and ~ 92 °C for EN AW-6082-T6. Notably, these temperatures are close to the PET glass transition temperature (T_g) which is approximately 80 °C [9,10,40,60,61]. At temperatures above the PET T_g , polymer chains acquire some mobility. According to a previous study [28], the adhesion strength of mechanical interlocking soars with increasing temperature because of the higher chains mobility. The viscosity temperature coefficient of a bottle-grade PET with an intrinsic viscosity of 0.85 ± 0.02 dl/g was recently measured [62] and it confirmed that molten PET viscosity falls sharply with polymer temperature increase.

Moreover, mechanical interlocking is a function of the contact surface roughness, which is similar for the two tested plates. The metal physical properties listed in Table 5 can help clarify this phenomenon.

The morphologies of the chromium oxide (Cr_2O_3) and of the aluminum oxide (Al_2O_3) layers are similar. Their thickness (few nanometers) is orders of magnitude lower than the cavities dimensions in which PET/metal mechanical interlocking can occur. Therefore, oxides influence on the thermal energy exchange is almost negligible.

The thermal conductivity of EN AW-6082-T6 is an order of

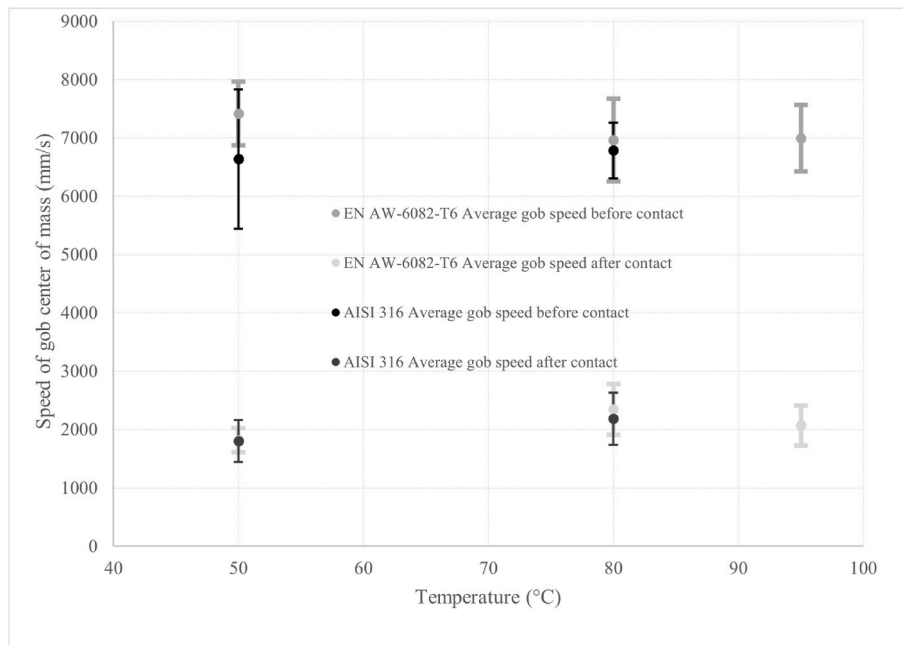


Fig. 7. Average gob speeds and their standard deviations obtained before and after the plate contact for different temperatures and plate materials. Gobs average speeds before contact are approximately 7000 mm/s and after contact they are approximately 2000 mm/s for each temperature and plate material.

Table 5

Physical properties of the EN AW-6082-T6 aluminum alloy, AISI 316 stainless steel and molten PET[63–65].

	Aluminum alloy EN AW-6082-T6	Stainless steel AISI 316	PET (molten state)
Elastic modulus (GPa)	70	186	–
Thermal conductivity [W/(m K)] at 23 °C (metals) or at 275 °C (PET)	170–220	16.3	0.23
Density [kg/m ³]	2700	8060	1200
Coefficient of thermal expansion [1/(10 ⁶ K)] at 23 °C	23.4	16–18	–
Specific heat [J/(kg K)]	896	502	1950
Thermal effusivity [J/(√s m ² K)] ^a	21720	8121	734
Thermal diffusivity [10 ^{−6} m ² /s] ^a	81	4	0.098

^a An average value was chosen as EN AW-6082-T6 thermal conductivity.

magnitude higher than that of AISI 316 and is three orders of magnitude higher than that of PET. Moreover, the thermal diffusivity of PET is much lower than that of the two metals, specifically forty-one times less than AISI 316 one and eight hundred and twenty times less than EN AW-6082-T6 one. Finally, PET thermal effusivity is eleven times less than AISI 316 one and thirty times less than EN AW-6082-T6 one. The result is that the superficial layer of the PET gob which touches the metal plate is quickly cooled down even below T_g .

The gob surface temperature after the contact with the EN AW-6082-T6 plate is lower than that after contact with AISI 316 because the first has an effusivity (i.e. the ability to exchange thermal energy with the gob) and a diffusivity (i.e. the ability to distribute the thermal energy coming from the gob to the rest of the plate) three and twenty times higher than the latter, respectively. Therefore, the lower temperature on the PET surface layer at the same plate temperature may be the reason for the different behaviors of the EN AW-6082-T6 and AISI 316 materials. For example, at a plate temperature of about 92 °C, the PET chain mobility is sufficiently high to induce mechanical interlocking on the AISI 316 surface but not on the EN AW-6082-T6 surface. Testing other materials with different thermal properties (such as copper or other types of steel) could help verify these conclusions in the future.

As previously stated, at temperatures ≥ 115 °C, all 49 gobs stuck on the EN AW-6082-T6 plate, while on the AISI 316 plate, one gob out of 63 bounced at approximately 116 °C and another at approximately 126 °C. The reason for this phenomenon remains unclear; thus, further investigation (for example examining the effect of other parameters, such as the different coefficient of thermal expansion) is required in this area.

4. Conclusion

In this study, the effect of the metal plate temperature on the short contact time (~ 3 ms, typical for compression molding) molten PET–metal adhesiveness was studied for the first time by creating more than 300 single contacts.

Two metal plates fabricated from different materials (AISI 316 and EN AW-6082-T6 that are widely used in the beverage industry) with similar surface roughness, morphology, and SFE values were employed for this purpose. The obtained results revealed that the gobs did not adhere to the metal plates below a specific metal temperature close to the T_g of PET. Its value determined for EN AW-6082-T6 was higher than that obtained for AISI 316 by 10–14 °C.

Approximate analysis of the energy values dissipated during contact at different plate temperatures indicated that the adhesion process followed the on–off mechanism.

Polymer chains acquire good mobility above T_g , which can lead to mechanical interlocking and can promote adhesion beyond a certain

threshold. The superficial layer of the PET gob that touches the metal plate is rapidly cooled, owing to the polymer thermal properties combined to the ones of the metal plate. Because the thermal effusivity, conductivity and diffusivity of EN AW-6082-T6 are approximately three times, ten times and twenty times, respectively, higher than that of AISI316, the aluminum alloy can freeze PET chains at higher plate temperatures, thus preventing the adhesion of the PET gob to the metal surface.

Therefore, EN AW-6082-T6 can be potentially used as a material for gob handling tools in industrial applications because, compared with AISI316, it can endure higher temperatures without causing any adhesion-related problems. Moreover, for single-contact adhesion, it is important to remain below a threshold temperature established for a particular metal and it seems not necessary to spend energy to maintain a precise plate temperature.

Future tests involving different materials could verify the proposed hypotheses. Moreover, it would be interesting to study the contribution of surface roughness to the short contact time adhesion, which was not considered in this study.

In summary, this is the first study on the short contact time PET–metal adhesion, and it elucidates its mechanism and clearly demonstrates the difference between the adhesion properties of the stainless steel AISI 316 and the aluminum alloy EN AW-6082-T6. The obtained results may strongly have an impact on PET compression molding technology and aid in the selection of materials and temperatures for component touching molten PET cylinders.

Finally, this research has a great scientific significance because it examines for the first time a phenomenon, the short contact time (milliseconds) plastic/metal adhesion, that is currently unknown to the scientific community and that could arouse an interest in many other research and industrial fields.

CRediT authorship contribution statement

Marco Carati: Conceptualization, Methodology, Validation, Formal analysis, Investigation, Resources, Writing – original draft, Writing – review & editing, Visualization, Funding acquisition. **Maurizio Fiorini:** Resources, Formal analysis, Supervision.

Declaration of competing interest

The authors declare the following financial interests/personal relationships which may be considered as potential competing interests: Marco Carati reports financial support was provided by Sacmi Imola S.C. Marco Carati reports a relationship with Sacmi Imola SC that includes: employment. Marco Carati has patent #European Patent 3512, Vol. 679 issued to SACMI Imola S.C. Maurizio Fiorini reports equipment, drugs, or supplies was provided by Sacmi Imola SC.

Data availability

The data that has been used is confidential.

Acknowledgments

This article originated from Marco Carati's doctoral dissertation [66] under the supervision of Professor Maurizio Fiorini. The authors would like to thank SACMI Imola S.C. for its material support and, last but not least, Ms. Debora Barnabé.

Nomenclature

IV	Intrinsic viscosity
PET	Poly(ethylene terephthalate)
PID	Proportional–integral–derivative
RH	Relative humidity

SBM	Stretch blow molding
SACMI	Società Anonima Cooperativa Meccanici Imola
SFE	Surface free energy
T _g	Glass transition temperature

References

- [1] V. Pandey, M. Seese, J.M. Maia, D.A. Schiraldi, Thermo-rheological analysis of various chain extended recycled poly(ethylene terephthalate), *Polym. Eng. Sci.* 60 (10) (2020) 2511–2516, <https://doi.org/10.1002/pen.25488>.
- [2] S.A. Jabarin, E.A. Logfren, Thermal stability of polyethylene terephthalate, *Polym. Eng. Sci.* 24 (13) (1984) 1056–1063, <https://doi.org/10.1002/pen.760241311>.
- [3] M. Cakmak, J.L. White, J.E. Spruiell, Optical properties of simultaneous biaxially stretched poly(ethylene terephthalate) films, *Polym. Eng. Sci.* 29 (21) (1989) 1534–1543, <https://doi.org/10.1002/pen.760292108>.
- [4] M. Evstatiev, S. Fakirov, A. Apostolov, H. Hristov, J.M. Schultz, Structure and mechanical properties of highly oriented poly(ethylene terephthalate) films, *Polym. Eng. Sci.* 32 (14) (1992) 964–970, <https://doi.org/10.1002/pen.760321408>.
- [5] P. Varma, E.A. Logfren, S.A. Jabarin, Properties and kinetics of thermally crystallized oriented poly(ethylene terephthalate) (PET). I: Kinetics of crystallization, *Polym. Eng. Sci.* 38 (2) (1998) 237–244, <https://doi.org/10.1002/pen.10184>.
- [6] S.A. Jabarin, Orientation of precrystallized poly(ethylene terephthalate), *Polym. Eng. Sci.* 31 (14) (1991) 1071–1078, <https://doi.org/10.1002/pen.760311412>.
- [7] S.A. Jabarin, Strain-induced crystallization of poly(ethylene terephthalate), *Polym. Eng. Sci.* 32 (18) (1992) 1341–1349, <https://doi.org/10.1002/pen.760321802>.
- [8] N. Wyeth, *Biaxially Oriented Poly(ethylene Terephthalate) Bottle*, vol. 309, U.S. Patent 3733, 1973.
- [9] M. Bordival, F.M. Schmidt, Y. Le Maout, V. Velay, Optimization of preform temperature distribution for the stretch-blow molding of PET bottles: infrared heating and blowing modeling, *Polym. Eng. Sci.* 49 (4) (2009) 783–793, <https://doi.org/10.1002/pen.21296>.
- [10] J. Zimmer, G. Chauvin, M. Stommel, Experimental investigation and numerical simulation of liquid supported stretch blow molding, *Polym. Eng. Sci.* 55 (4) (2015) 933–944, <https://doi.org/10.1002/pen.23961>.
- [11] D. Marastoni, *SACMI heroPET4.0, Connecting comPETence*, vol. 3, 2016, pp. 42–46.
- [12] P.A.M. Sacmi, (PREFORM advanced moulding) production of compression preforms. <https://www.sacmi.com/en-US/Food-Beverage/Beverage/PAM>, 2023. (Accessed 23 October 2023).
- [13] C. Bonnebat, G. Roulet, A.J. de Vries, Biaxially oriented poly(ethylene terephthalate) bottles: effects of resin molecular weight on parison stretching behavior, *Polym. Eng. Sci.* 21 (4) (1981) 189–195, <https://doi.org/10.1002/pen.760210403>.
- [14] S.A. Jabarin, Orientation studies of poly(ethylene terephthalate), *Polym. Eng. Sci.* 24 (5) (1984) 376–384, <https://doi.org/10.1002/pen.760240513>.
- [15] K. Takeuchi, T. Kurosawa, K. Ichikawa, N. Hirota, *European Patent 1849 573* (2013).
- [16] Y. Asano, N. Hirota, J. Nagao, K. Watanabe, *European Patent 1985 430* (2012).
- [17] Y. Asano, N. Hirota, J. Nagao, K. Watanabe, *European Patent 2404 732* (2017).
- [18] G.A. Ritz, T.C. Truman, *European Patent 1742 783* (2005).
- [19] O. Dos Santos Ferreira, A. Stevens, C. Schrauwen, Quantitative comparison of adhesion in metal-to-plastic systems, *Thin Solid Films* 517 (10) (2009) 3070–3074, <https://doi.org/10.1016/j.tsf.2008.11.117>.
- [20] D. Marastoni, M. Carati, *European Patent 3512 679* (2017).
- [21] G. Kafkopoulos, C.J. Padberg, J. Duvigean, G.J. Vancso, Adhesion engineering in polymer metal Comolded joints with biomimetic polydopamine, *ACS Appl. Mater. Interfaces* 13 (2021) 19244–19253, <https://doi.org/10.1021/acami.1c01070>.
- [22] S. Yin, Y. Xie, R. Li, J. Zhang, T. Zhou, Polymer-metal hybrid material with an ultra-high interface strength based on mechanical interlocking via nanopores produced by electrochemistry, *Ind. Eng. Chem. Res.* 59 (2020) 12409–12420, <https://doi.org/10.1021/acs.iecr.0c01304>.
- [23] S. Mousa, A. G-Y Kim, Direct adhesion of metal-polymer metal sandwich composites by warm roll bonding, *J. Mater. Process. Technol.* 239 (2017) 133–139, <https://doi.org/10.1016/j.jmatprotec.2016.08.017>.
- [24] R.L. Vasconcelos, G.H.M. Oliveira, S.T. Amancio-Filho, L.B. Canto, Injection overmolding of polymer-metal hybrid structures: a review, *Polym. Eng. Sci.* 63 (2023) 691–722, <https://doi.org/10.1002/pen.26244>.
- [25] S. Zhang, X. Zeng, Z. Tang, M.J. Tan, Exploring the antisticking properties of solid lubricant thin films in transfer molding, *Int. J. Mod. Phys. B* 16 (2002) 1080–1085, <https://doi.org/10.1142/S0217979202010890>.
- [26] K.V. Shalnov, K. Uemura, Y. Ito, Consideration on surface modification of steel dies to reducing the plastic sticking in the forming process, *Tribol. Online* 7 (3) (2012) 190–200, <https://doi.org/10.2474/trol.7.190>.
- [27] J.V. Chen, S.J. Hwang, Application of surface treatments on releasing adhesion force during thermoplastic polyurethane injection molding process, *Polym. Eng. Sci.* 57 (3) (2017) 299–305, <https://doi.org/10.1002/pen.24413>.
- [28] K. Ramani, B. Moriarty, Thermoplastic bonding to metals via injection molding for macro-composite manufacture, *Polym. Eng. Sci.* 38 (5) (1998) 870–877, <https://doi.org/10.1002/pen.10253>.
- [29] M. Kono, *Studies of Metal-Polymer Interface* (PhD Thesis), University of British Columbia, 2000.
- [30] S. Petit, P. Laurens, M.G. Barthes-Labrousse, J. Amouroux, F. Aréfi-Khonsari, Al/PET adhesion: role of an excimer laser pretreatment of PET prior to aluminum thermal evaporation, *J. Adhes. Sci. Technol.* 17 (3) (2003) 353–368, <https://doi.org/10.1163/156856103762864660>.
- [31] J.F. Silvain, J.J. Ehrhardt, An overview on metal/PET adhesion, *Thin Solid Films* 236 (1–2) (1993) 230–235, [https://doi.org/10.1016/0040-6090\(93\)90675-F](https://doi.org/10.1016/0040-6090(93)90675-F).
- [32] J.F. Silvain, A. Veyrat, J.J. Ehrhardt, Effect of the temperature on the adhesion and the morphology of thin metal films evaporated on polyethylene terephthalate, *Thin Solid Films* 221 (1–2) (1992) 114, [https://doi.org/10.1016/0040-6090\(92\)90803-J](https://doi.org/10.1016/0040-6090(92)90803-J).
- [33] E. Zumelzu, F. Rull, P. Schmidt, A.A. Boettcher, Structural analysis of polymer-metal laminates by electron microscopy and infrared spectroscopy, *Surf. Coat. Int. B Coat. Trans.* 89 (1) (2006) 57–62, <https://doi.org/10.1007/BF02699615>.
- [34] E. Zumelzu, C. Angulo, C. Cabezas, R. Ugarte, Characterisation of nanometric chromium coatings in metal-polymer composites, *Surf. Eng.* 29 (8) (2013) 620–626, <https://doi.org/10.1179/1743294413Y.0000000160>.
- [35] F.M. De Wit, Ö. Özkanat, J.M.C. Mol, H. Terryn, J.H.W. Dewit, The influence of pre-treatments of aluminium alloys on bonding of PET coatings, *Surf. Interface Anal.* 42 (4) (2010) 316–320, <https://doi.org/10.1002/sia.3228>.
- [36] L. Bratt, *Fish Canning Handbook*, Wiley, Blackwell, NJ, 2010.
- [37] T.A. Turner, *Canmaking for Can Fillers*, CRC Press, FL, 2001.
- [38] H. Al-Maliki, L. Zsidai, P. Samyn, Z. Szakal, R. Keresztes, G. Kalacska, Effects of atmospheric plasma treatment on adhesion and tribology of aromatic thermoplastic polymers, *Polym. Eng. Sci.* 58 (S1) (2018) E93–E103, <https://doi.org/10.1002/pen.24689>.
- [39] Z. Bashir, I. Al-Aloush, I. Al-Raqibah, M. Ibrahim, Evaluation of three methods for the measurement of crystallinity of pet resins, preforms, and bottles, *Polym. Eng. Sci.* 40 (11) (2000) 2442–2455, <https://doi.org/10.1002/pen.11376>.
- [40] M. Vigny, A. Aubert, J.M. Hiver, M. Aboulfaraj, C. G'Sell, Constitutive viscoplastic behavior of amorphous PET during plane-strain tensile stretching, *Polym. Eng. Sci.* 39 (12) (1999) 2366–2376, <https://doi.org/10.1002/pen.11625>.
- [41] S. Tang, N. Lu, S.W. Myung, H.S. Choi, Enhancement of adhesion strength between two AISI 316 L stainless steel plates through atmospheric pressure plasma treatment, *Surf. Coat. Tech.* 200 (2006) 5220–5228, <https://doi.org/10.1016/j.surfcoat.2005.06.020>.
- [42] A. Rudawska, *Surface Treatment in Bonding Technology*, Academic Press, UK, 2019, <https://doi.org/10.1016/C2018-0-01281-5>.
- [43] D.H. Kaelble, Dispersion-polar surface tension properties of organic solids, *J. Adhes. 2* (2) (1970) 66–81, <https://doi.org/10.1080/0021846708544582>.
- [44] D.K. Owens, R.C. Wendt, Estimation of the surface free energy of polymers, *J. Appl. Polym. Sci.* 13 (8) (1969) 1741, <https://doi.org/10.1002/app.1969.070130815>.
- [45] W. Rabel, *Einige Aspekte der Benetzungstheorie und ihre Anwendung auf die Untersuchung und Veränderung der Oberflächeneigenschaften von Polymeren, Farbe Lack* 77 (1971) 997–1005.
- [46] M. Zenkiewicz, Wettability and surface free energy of corona-treated biaxially-oriented polypropylene film, *J. Adhes. Sci. Technol.* 15 (14) (2001) 1769–1785, <https://doi.org/10.1163/15685610152715773>.
- [47] S. Shaleh-Levanon, A. Marmur, Validity and accuracy in evaluating surface tension of solids by additive approaches, *J. Colloid Interface Sci.* 262 (2) (2003) 489–499, [https://doi.org/10.1016/S0021-9797\(02\)00231-X](https://doi.org/10.1016/S0021-9797(02)00231-X).
- [48] A. Rudawska, Surface free energy and 7075 aluminium bonded joint strength following degreasing only and without any prior treatment, *J. Adhes. Sci. Technol.* 26 (2012) 1233–1247, <https://doi.org/10.1163/156856111X593577>.
- [49] K.J. Kubiak, M.C.T. Wilson, T.G. Mathia, P. Carval, Wettability versus roughness of engineering surfaces, *Wear* 271 (3–4) (2011) 523–528, <https://doi.org/10.1016/j.wear.2010.03.029>.
- [50] J.D. Bernardin, I. Mudawar, C.B. Walsh, E.I. Franses, Contact angle temperature dependence for water droplets on practical aluminum surfaces, *Int. J. Heat Mass Transfer* 40 (5) (1997) 1017–1033, [https://doi.org/10.1016/0017-9310\(96\)00184-6](https://doi.org/10.1016/0017-9310(96)00184-6).
- [51] J.W. Song, L.W. Fan, Temperature dependence of the contact angle of water: a review of research progress, theoretical understanding, and implications for boiling heat transfer, *Adv. Colloid Interface Sci.* 288 (2021), 102339, <https://doi.org/10.1016/j.cis.2020.102339>.
- [52] X. Zou, K. Chen, H. Yao, C. Chen, X. Lu, P. Ding, M. Wang, X. Hua, A. Shan, Chemical reaction and bonding mechanism at the Polymer–Metal interface, *ACS Appl. Mater. Interfaces* 14 (2022) 27383–27396, <https://doi.org/10.1021/acami.2c04971>.
- [53] J.M. Dealy, J. Wang, *Melt Rheology and its Applications in the Plastic Industry*, second ed., Springer, Netherlands, 2013 <https://doi.org/10.1007/978-94-007-6395-1>.
- [54] B.K. Kim, H.M. Jeong, Y.H. Lee, Melt rheology of poly(ethylene terephthalate), polyarylate, and their blends, *J. Appl. Polym. Sci.* 40 (11–12) (1990) 1805–1818, <https://doi.org/10.1002/app.1990.070401101>.
- [55] J.S. Forsythe, L. Cheah, D.R. Nisbet, R.K. Gupta, A. Lau, A.R. Donovan, M. S. O'Shea, G. Moad, Rheological properties of high melt strength poly(ethylene terephthalate) formed by reactive extrusion, *J. Appl. Polym. Sci.* 100 (5) (2006) 3646–3652, <https://doi.org/10.1002/app.23166>.
- [56] M. Kruse, M.H. Wagner, Time-resolved rheometry of poly(ethylene terephthalate) during thermal and thermo-oxidative degradation, *Rheol. Acta* 55 (2016) 789–800, <https://doi.org/10.1007/s00397-016-0955-2>.
- [57] R.R. Chowreddy, K. Nord-Varhaug, F. Rapp, Recycled polyethylene terephthalate/carbon nanotube composites with improved processability and performance, *J. Mater. Sci.* 53 (9) (2018) 7017–7029, <https://doi.org/10.1007/s10853-018-2014-0>.

- [58] D.W. Green, R.H. Perry, *Perry's Chemical Engineers' Handbook*, McGraw-Hill, NY, 2008.
- [59] T. Okada, R. Ishige, S. Ando, Analysis of thermal radiation properties of polyimide and polymeric materials based on ATR-IR spectroscopy, *J. Photopolym. Sci. Technol.* 29 (2) (2016) 251–254, <https://doi.org/10.2494/photopolymer.29.251>.
- [60] D. Chen, H.G. Zachmann, Glass transition temperature of copolyesters of PET, PEN and PHB as determined by dynamic mechanical analysis, *Polymer* 32 (9) (1991) 1612–1621, [https://doi.org/10.1016/0032-3861\(91\)90396-Z](https://doi.org/10.1016/0032-3861(91)90396-Z).
- [61] B.U. Durmaz, C. Ozturk, A. Aytac, Reduced graphene oxide reinforced PET/PBT nanocomposites: Compatibilization and characterization, *Polym. Eng. Sci.* 60 (10) (2020) 2606–2618, <https://doi.org/10.1002/pen.25498>.
- [62] D.S.C. Andrade, L.E. Canedo, L.H. de Carvalho, R. Barbosa, T.S. Alves, Characterization of poly(ethylene terephthalate) by torque rheometry, *Mater. Res.* 24 (2) (2021) 238–245, <https://doi.org/10.1590/1980-5373-MR-2020-0238>.
- [63] <http://www.totalmateria.com>, 2017. (Accessed 15 October 2017).
- [64] <http://www.goodfellow.com>, 2020. (Accessed 29 December 2020).
- [65] C.M.A. Lopes, M.I. Felisberti, Thermal conductivity of PET/(LDPE/Al) composites determined by MDSC, *Polym. Test.* 23 (6) (2004) 637–643, <https://doi.org/10.1016/j.polymertesting.2004.01.013>.
- [66] M. Carati, *Handling of Molten Poly(ethylene Terephthalate) Cylinders for Preforms Compression Molding Machines* (PhD Thesis), Alma Mater Studiorum University of Bologna, Italy, 2018.